Supporting information

Selenium-doped hematite (α-Fe_2O_3) hollow nanorods for highly sensitive and selective detection of trace NO_2

Tingting Liang,[a,c] *Yan Li,*[a] *Xu Zhang,*[a] *Hongwei Bao,* [a] *Fengnan Li,*[d] *Xueqian Liu,* [b] *Zhengfei Dai,*[a] *and Hang Liu* [a,b*]

[a] State Key Laboratory for Mechanical Behavior of Materials, Xi'an Jiaotong University, Xi'an 710049, China

[b] Superconducting Materials Research Center, Northwest Institute for Non-ferrous Metal Research, Xi'an 710016, China

[c] School of Materials Science and Engineering, Henan University of Science and Technology, Luoyang 471023, China

[d] Institute of wide band gap semiconductors, Xi'an Jiaotong University, Xi'an 710049, China

*Corresponding author: liuhangnwpu@gmail.com

S1. Calculation of the detection limit of the gas sensor:

The detection limit of this Se-Fe_2O_3 sensor can be calculated as follows:

$$S = AC^{\beta} + 1 \quad (1)$$

Where A is the constant, C is the concentration of the target gas with the unit of ppm. The power exponent β is the parameter (usually from 0.5 to 1) depending on the charge of the surface species and the stoichiometry of the elementary reactions on the surface. When the relationship between the sensing signals and the concentrations is linear (shown in Fig. 4f), the Eqn. (1) can be written as:

$$S = 0.89 \times C + 1 \quad (2)$$

Therefore, the potential detection limit can be predicted from the Eqn. (2). If there is no noise, a slight change of the acquired signal can validate the existence of a gas when the ambient atmosphere is unchanged. Here, the detectable lower limit of the target gas concentration can be reasonably predicted on basis of the present signal-to-noise ratio. In Fig.4 (e), the noise signal N is found to be ~ 0.008. The standard requirement of the detection limit is (S-1)/N>3. Consequently, the response signal must be larger than 0.024 or the value of the sensing signal must be >1.024. From the Eqn. (2), the corresponding concentration can be estimated to be ~ 27 ppb with a signal of 1.024 when the drift of the sensor baseline is significantly lower. It means the detection limit of concentration to NO_2 is ~ 27 ppb at 130 °C.

S2. Electrical humidity sensing test:

The humidity sensing properties were tested in a home-built dynamic sensing system with gas flow controllers (500 sccm). The different humidity was generated by mixing the dry air and wet air (from saturated K_2SO_4 solution, 60%RH). The electrical resistance of sensing device was measured by Keithley DMM6500 digital multimeter. The humidity response was calculated by the value of R_{humid}/R_{air}, where R_{air} and R_{humid} are the sensor resistance under air and humid ambient.

Figure S1 Tingting Liang et al.

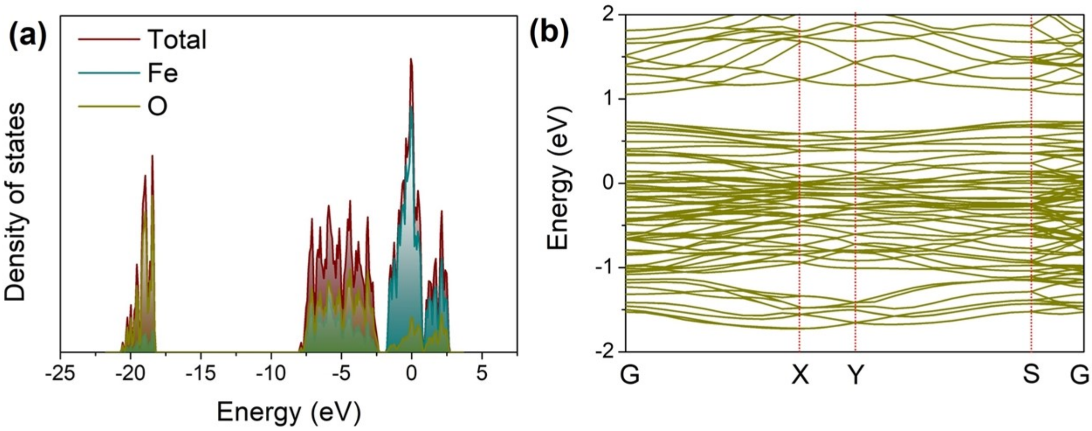

Fig. S1 (a) DOS and (b) band curves of Fe_2O_3.

Figure S2 Tingting Liang et al.

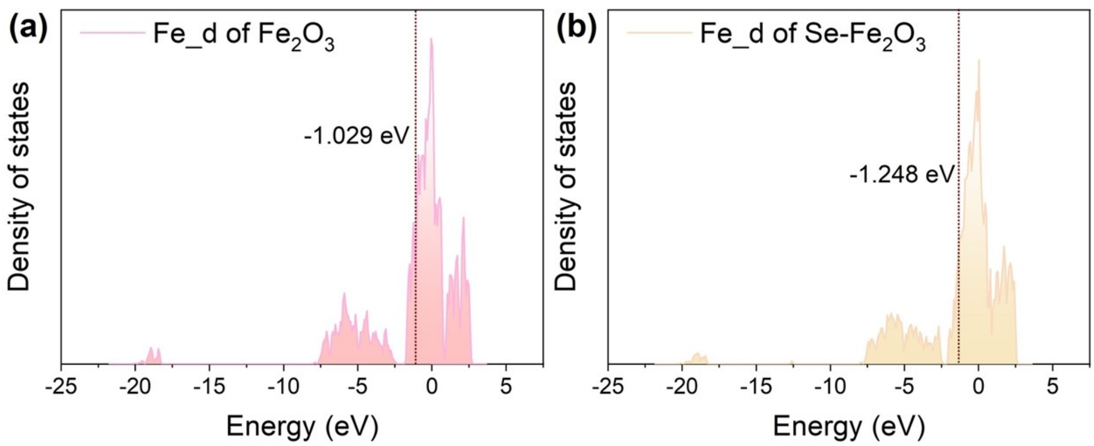

Fig. S2 The d-band centers of the Fe site in (a) Fe_2O_3 and (b) Se- Fe_2O_3.

Figure S3 Tingting Liang et al.

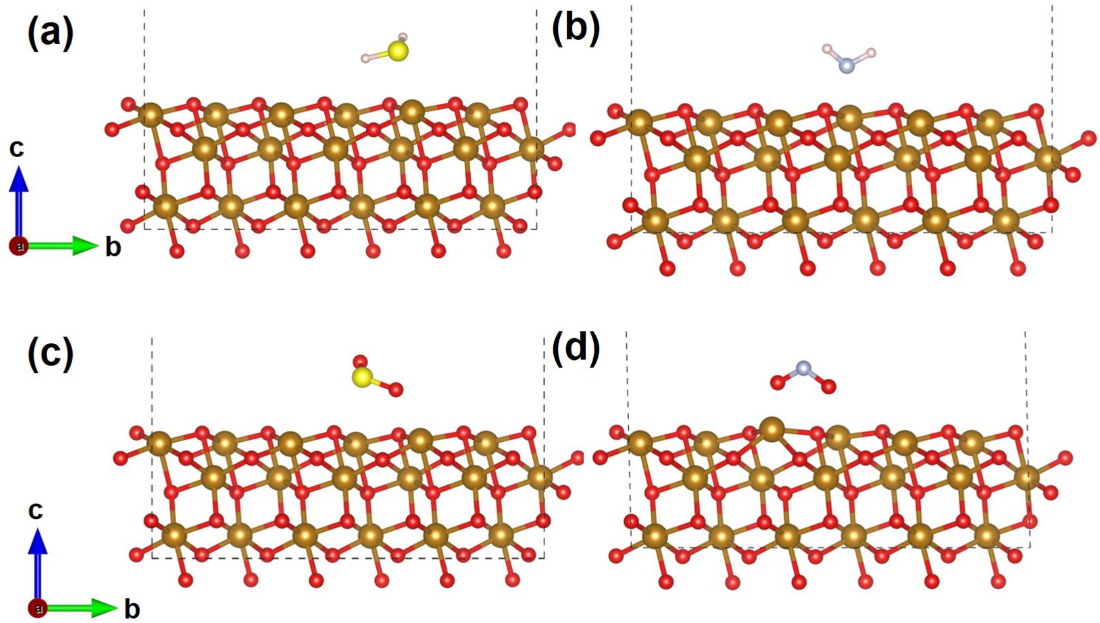

Fig. S3 The systems adsorbed with four kinds of gases on the surface of Fe_2O_3: (a) H_2S, (b) NH_3, (c) SO_2, and (d) NO_2, respectively.

Figure S4 Tingting Liang et al.

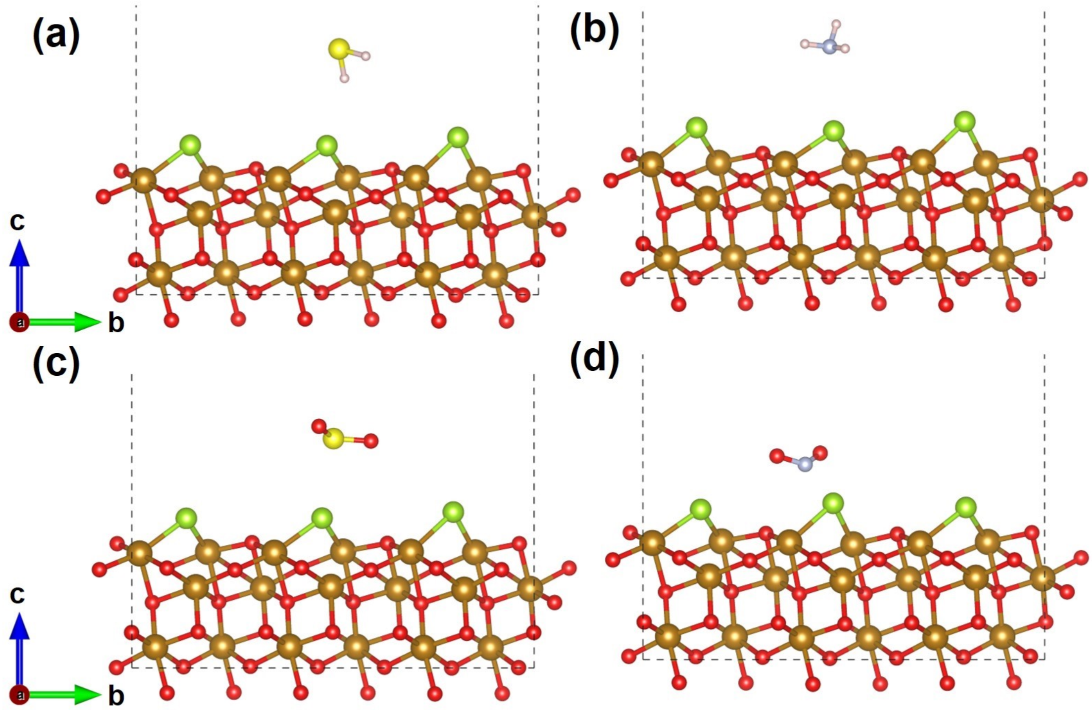

Fig. S4 The systems adsorbed with four kinds of gases on the surface of Se-Fe_2O_3: (a) H_2S, (b) NH_3, (c) SO_2, and (d) NO_2, respectively.

Table S1. The details of DFT calculation values of adsorption energies of each systems.

System	gas	$E_{DFT}^{gas^*}$ (eV)	E_{DFT}^{*}(eV)	$E_{DFT}^{gas(g)}$ (eV)	ΔE_{gas^*} (eV)
Fe_2O_3	H_2S	-462.85507	-451.04389	-11.251118	-0.56006
	NH_3	-471.55893	-451.04389	-19.57326	-0.94178
	SO_2	-468.70645	-451.04389	-17.167812	-0.49475
	NO_2	-471.01165	-451.04389	-18.429656	-1.5381
Se- Fe_2O_3	H_2S	-453.27378	-440.69052	-11.251118	-1.33214
	NH_3	-461.55718	-440.69052	-19.57326	-1.2934
	SO_2	-459.27424	-440.69052	-17.167812	-1.41591
	NO_2	-460.98534	-440.69052	-18.429656	**-1.86516**

Figure S5 Tingting Liang et al.

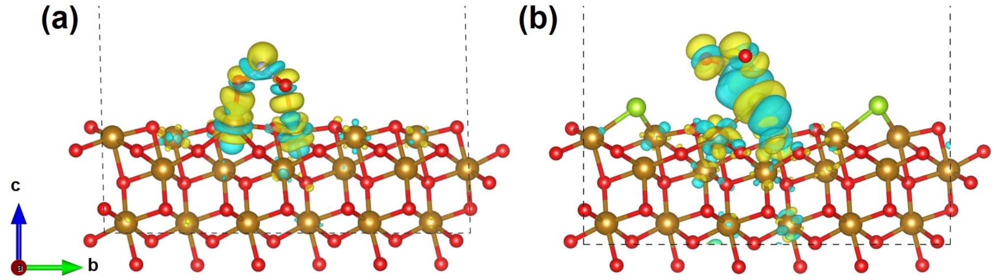

Fig. S5 Bader distribution of the systems adsorbed with NO_2 on the (a) Fe_2O_3 and (b) Se-Fe_2O_3, respectively.

Table S2. Doping content of Se in the Se-Fe_2O_3 samples obtained from ICP-MS tests.

Items information		Sample number		
		Se-Fe_2O_3-1	Se-Fe_2O_3-2	Se-Fe_2O_3-3
Se	mol %	0.8 %	1.0 %	1.6 %

Figure S6 Tingting Liang et al.

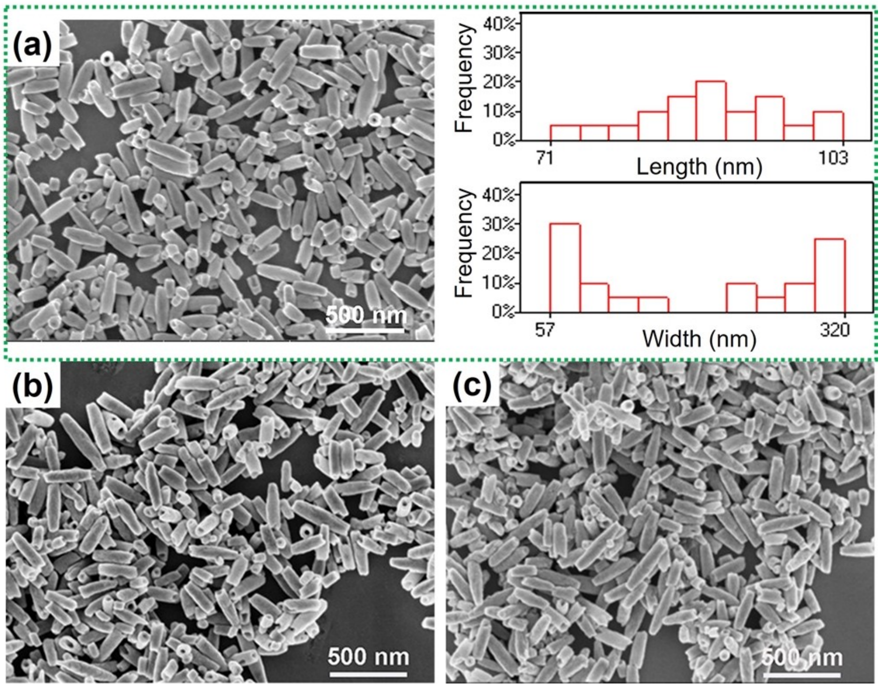

Fig. S6 The SEM images of (a) Fe_2O_3 (the right panels are histogram distribution of the length and the width of the nanorod), (b) Se-Fe_2O_3-1, and (c) Se-Fe_2O_3-3, respectively.

Figure S7 Tingting Liang et al.

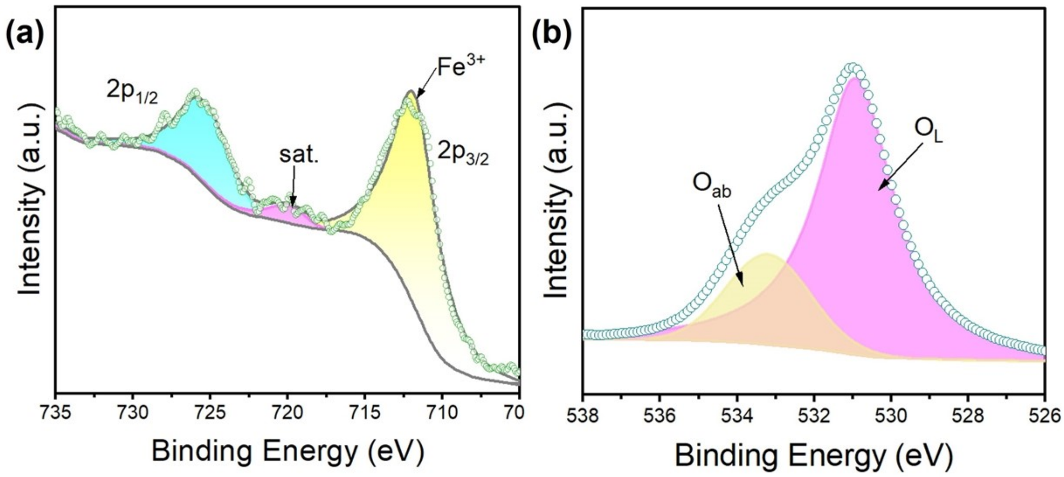

Fig. S7 XPS spectra of (a) Fe 2p and (b) O 1s of the Fe_2O_3 hollow nanorods.

Figure S8 Tingting Liang et al.

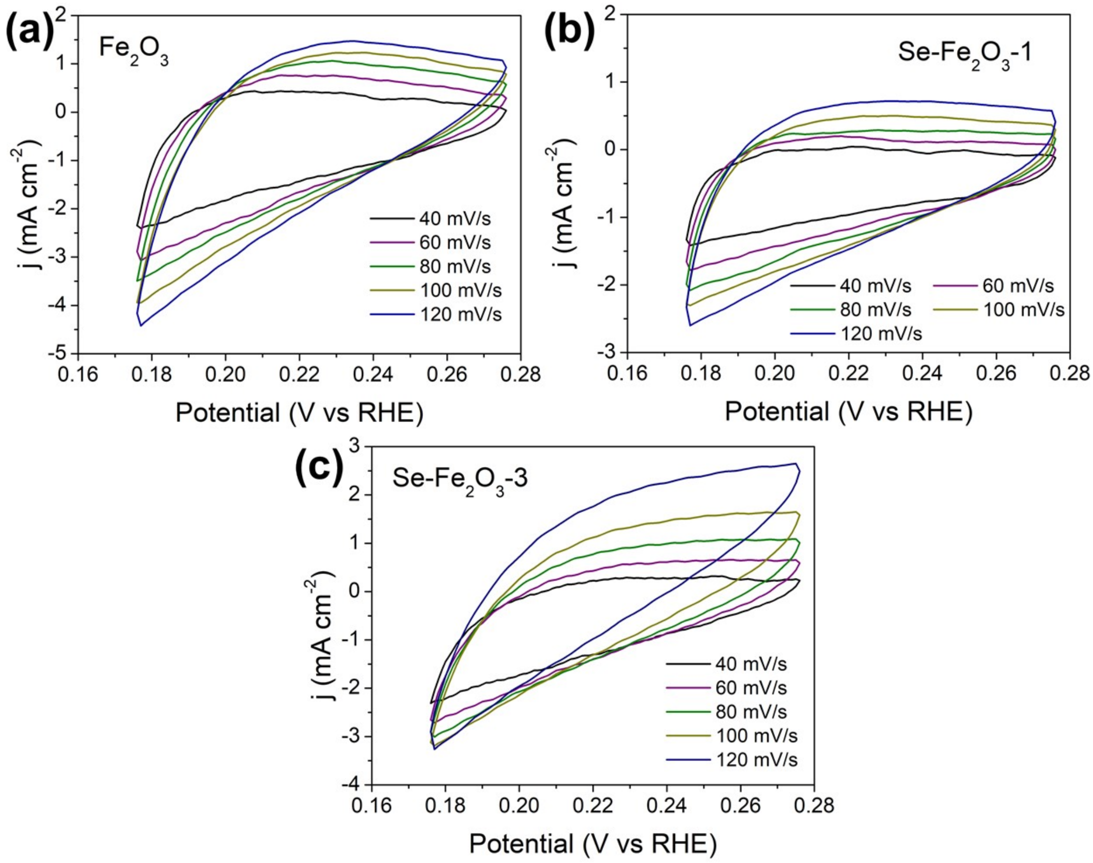

Fig. S8 CV curves of the samples: (a) Fe_2O_3, (b) $Se-Fe_2O_3-1$, and (c) $Se-Fe_2O_3-3$.

Figure S9 Tingting Liang et al.

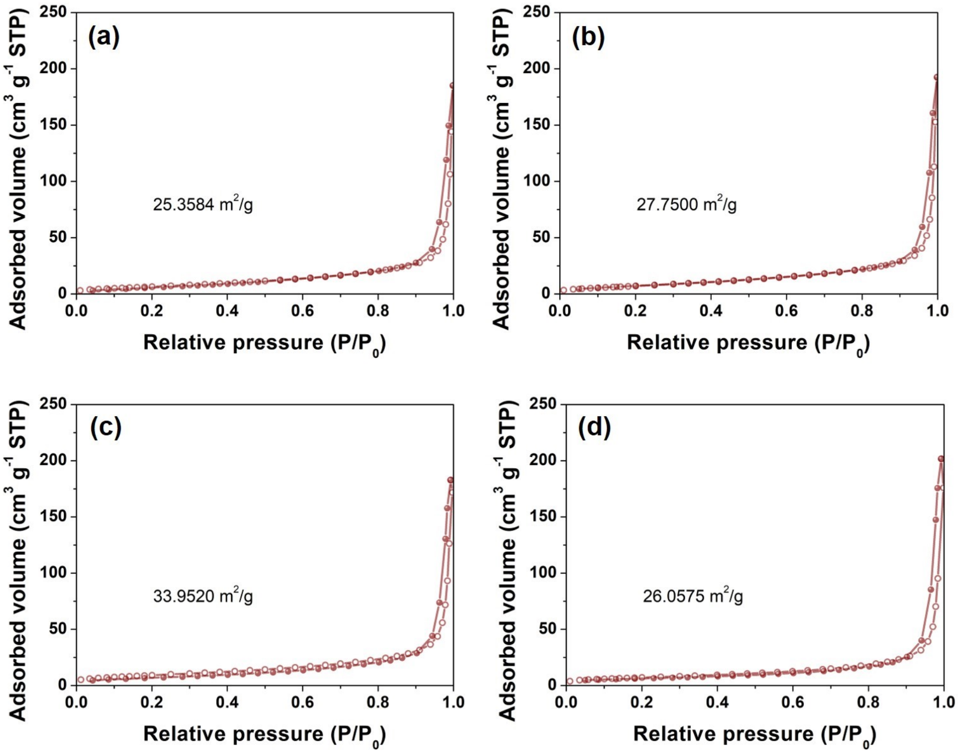

Fig. S9 The BET data of the (a) Fe_2O_3, (b) Se-Fe_2O_3-1, (c) Se-Fe_2O_3-2, and (d) Se-Fe_2O_3-3, respectively.

Figure S10 Tingting Liang et al.

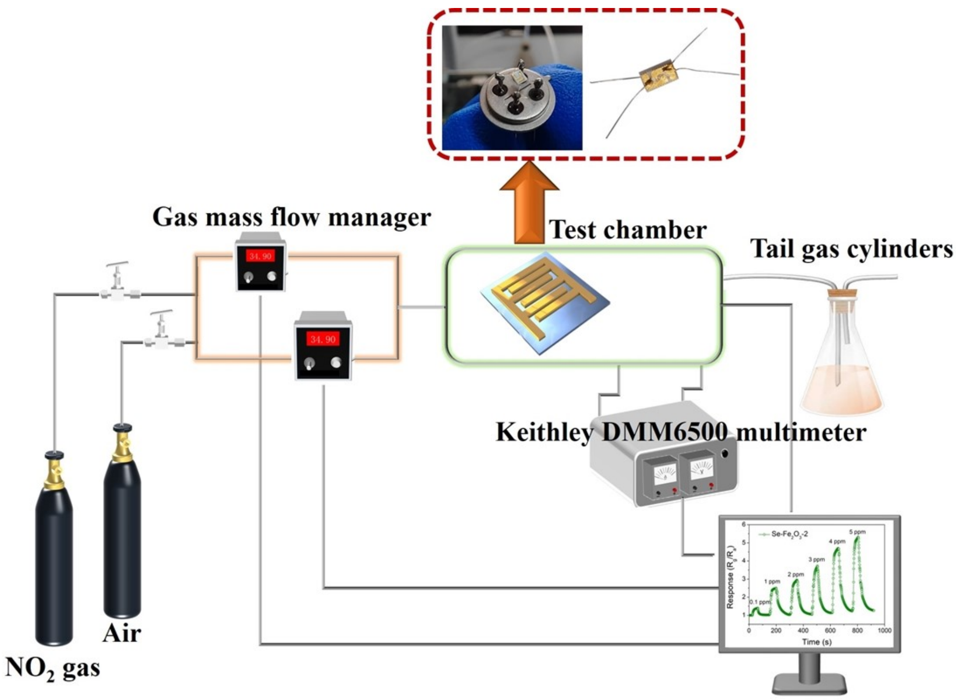

Fig. S10 The schematic diagram of the dynamic gas sensing test process.

Figure S11 Tingting Liang et al.

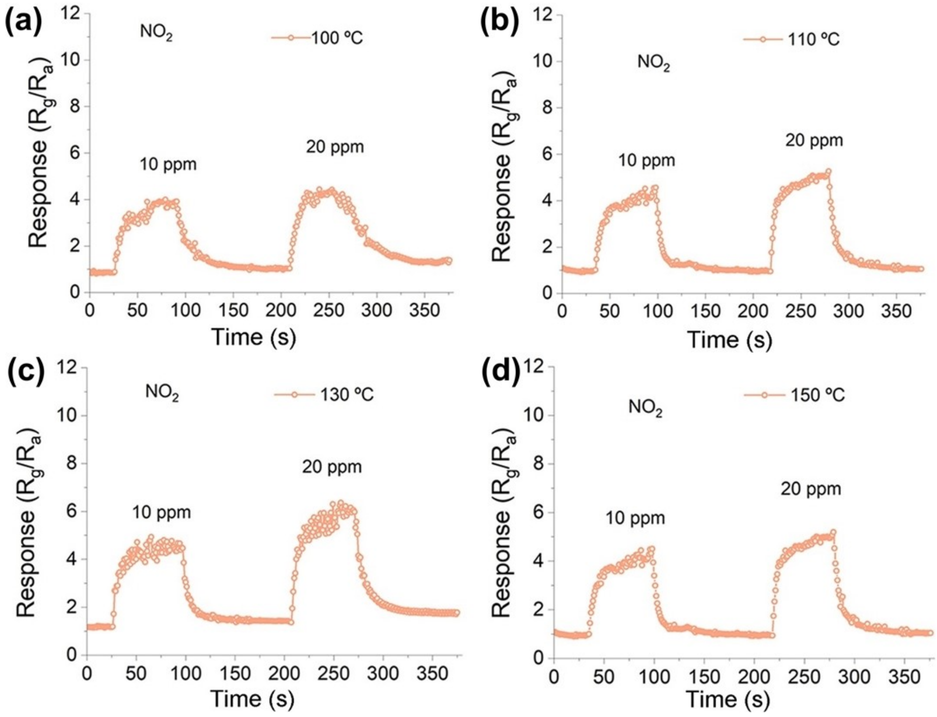

Fig. S11 The response of the Fe_2O_3 nanorods at different temperature: (a) 100 ℃, (b) 110 ℃, (c) 130 ℃, and (d) 150 ℃, respectively.

Figure S12 Tingting Liang et al.

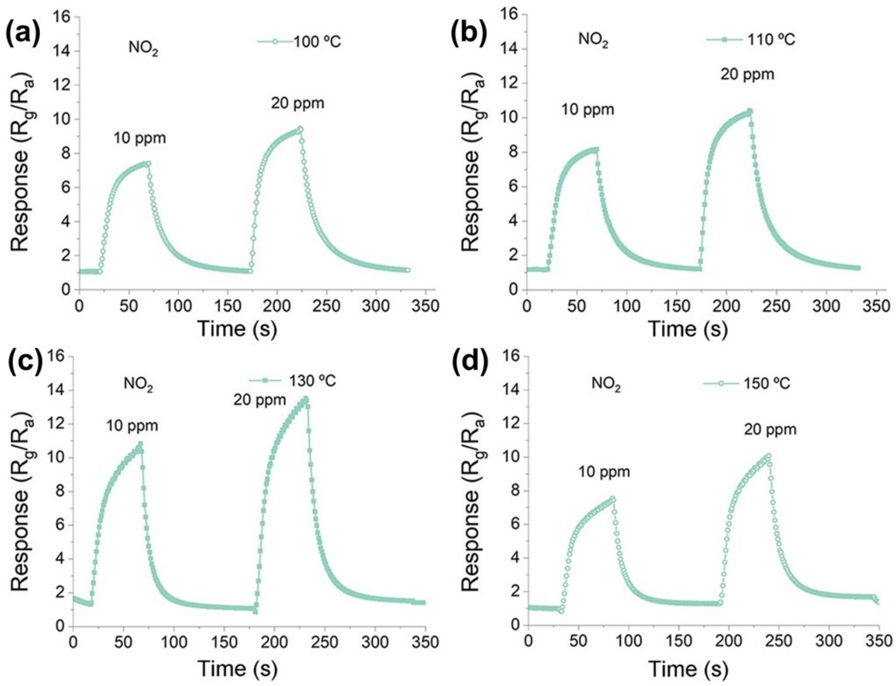

Fig. S12 The response of the Se-Fe_2O_3-1 sample at different temperature: (a) 100 ℃, (b) 110 ℃, (c) 130 ℃, and (d) 150 ℃, respectively.

Figure S13 Tingting Liang et al.

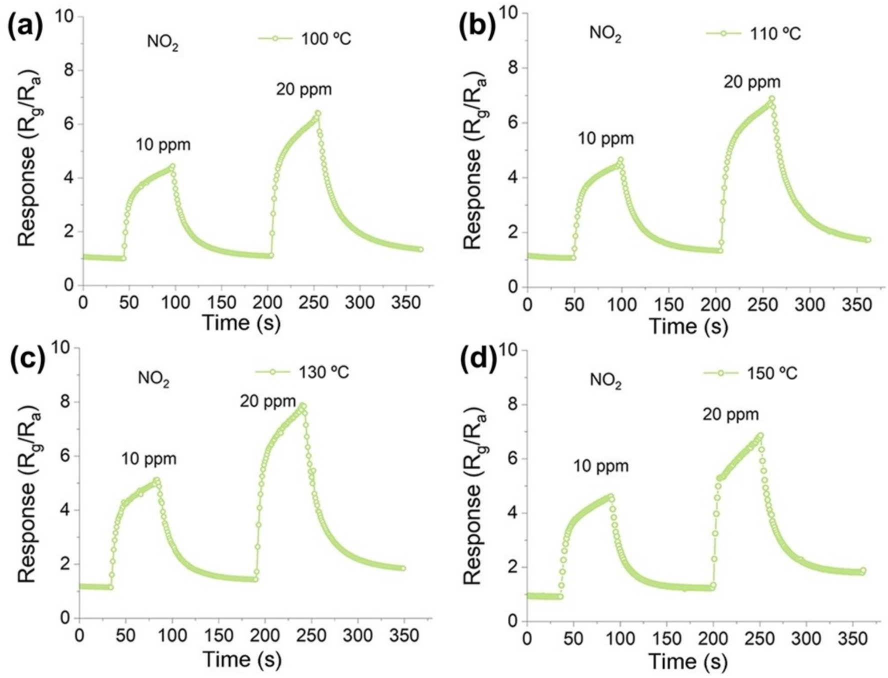

Fig. S13 The response of the Se-Fe_2O_3-3 sample at different temperature: (a) 100 °C, (b) 110 °C, (c) 130 °C, and (d) 150 °C, respectively.

Table S3. Comparison of response values of Fe_2O_3 and Se-Fe_2O_3 samples under 10 and 20 ppm NO_2.

	100 °C		110 °C		130 °C		150 °C	
Unit: ppm	10	20	10	20	10	20	10	20
Fe_2O_3	4	4.5	4.3	5.1	4.8	6.0	4.2	5.1
Se-Fe_2O_3-1	7.3	9.3	8.2	10.4	10.7	13.3	7.4	10.0
Se-Fe_2O_3-2	8.7	9.4	9.3	14.3	11.3	17.1	8.0	10.6
Se-Fe_2O_3-3	4.3	6.4	4.4	6.7	5.1	7.8	4.6	6.8

Table S4. Comparison of sensing performance based on the nanostructures towards NO_2 gas sensing in the previous literatures.

Sample	NO_2(ppm)	T (℃)	Rg/Ra	t_{res}/t_{rec} (s/s)	LOD(ppb)	Ref
Ag-Fe_2O_3@MoS_2	10	120	230.1%①	140/332	1	1
Cu-Fe_2O_3	50	300	2.59	110/278	5000	2
ZnO/α-Fe_2O_3	20	175	54	26/185	79	3
α-Fe_2O_3/$BiVO_4$	2	110	7.8	-----	500	4
α-Fe_2O_3-RGO	1	RT	3.1	472/2826	-----	5
γ-Fe_2O_3@RGO	100	200	6.86	1.25/--	100	6
Se-Fe_2O_3	**10**	**130**	**11.3**	**7/14**	**27**	**Present work**

① S=|Ra–Rg|/Ra×100% or S=|Rg–Ra|/Ra×100%

Figure S14 Tingting Liang et al.

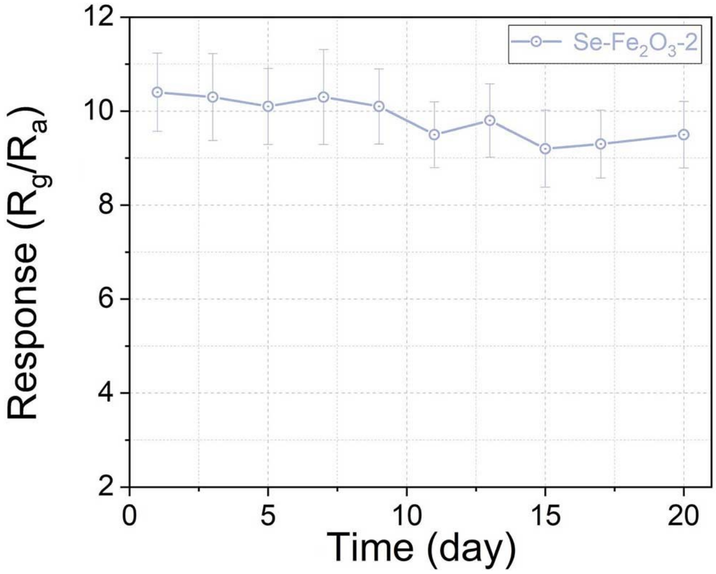

Fig. S14 The long-time stability test of the Se-Fe_2O_3-2 sample for 20 days.

Figure S15 Tingting Liang et al.

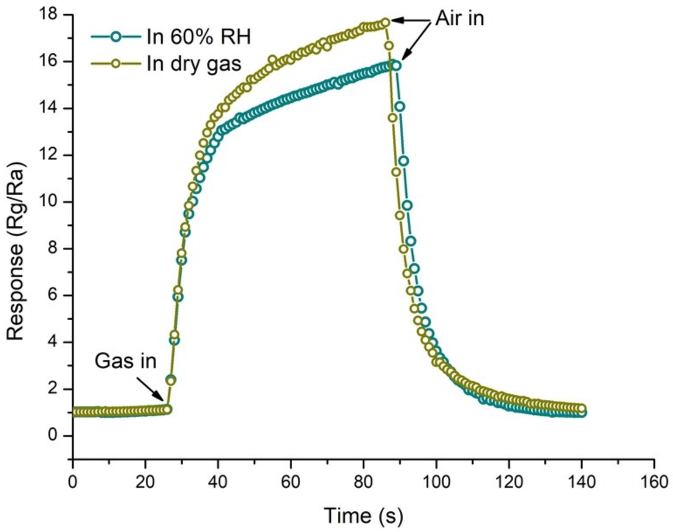

Fig. S15 The response of the Se-Fe_2O_3-2 sample under dry air and wet air background, respectively.

References

1 M. Yin, Y. Wang, L. Yu, H. Wang, Y. Zhu, C. Li, *J. Alloy. Compd.*, 2020, 829, 154471.

2 R. Wu, C. Lin, W. Tseng, *Ceram.Int.*, 2017, 43, S535-S540.

3 S. C. Zhang, L. H. Zhou, Y. H. Hu, X. H. Liu, J. Zhang, *Sens. Actuators B Chem.*, 2023, 396.

4 S. Bai, K. Tian, H. Fu, Y. Feng, R. Luo, D. Li, A. Chen, C. C. Liu, *Sens. Actuators B Chem.*, 2018, 136-143.

5 Y. Zhang, Z. Yang, L. Zhao, T. Fei, S. Liu, T. Zhang, *J. Colloid Interface Sci.*, 2022, 612, 689-700.

6 C. Zou, J. Hu, Y. J. Su, Z. H. Zhou, B. F. Cai, Z. J. Tao, T. T. Huo, N. T. Huo, Y. F. Zhang, *Sens. Actuators B Chem.*, 2020, 306, 127546.